Inversion of Upper Ocean Temperature Time Series for Entrainment, Advection, and Diffusivity

ALEXANDER G. OSTROVSKII

Frontier Observational Research System for Global Change, JAMSTEC, Tokyo, Japan

LEONID I. PITERBARG

Center for Applied Mathematical Sciences, University of Southern California, Los Angeles, California, and P.P. Shirshov Institute of Oceanography, Russian Academy of Sciences, Moscow, Russia

7 October 1998 and 16 June 1999

ABSTRACT

An inversion technique for estimating the terms of the oceanic near-surface heat transport is extended to include the vertical heat flux at the bottom of the surface mixed layer. The mixed-layer heat balance equation uses a conventional parameterization of the vertical heat flux via entrainment into the mixed layer of interior fluid during the mixed layer deepening. A heat conservation equation defined here for the sea temperature anomalies, deviations from the annual cycle, is driven by stochastic atmospheric forcing, thereby becoming essentially a stochastic partial differential equation. This equation is reduced to the regression estimator aimed on inversion of the sea temperature time series for the unknowns: vertical entrainment velocity, horizontal velocity and diffusivity, feedback factor, and atmospheric forcing parameter. The inversion scheme also involves the velocity divergence norm. The regression estimator is applied to the time series of vertical profiles of temperature anomalies compiled from the Comprehensive Ocean–Atmosphere Data Sets and the World Ocean Atlas 1994 on a 10-day mean basis over the spatial grid of 1° latitude × 2° longitude in two regions of the North Pacific: 1) near the ocean western boundary east of Japan and 2) between the Hawaiian islands and California. The inversion is implemented for winter data (December–March) from 1965 to 1990. The entrainment velocities are found to be of the order of 10^{-5} m s^{-1}. The entrainment effect is particularly significant in the Kuroshio–Oyashio frontal zone. The model skill is also substantially enhanced in this region: the inversion yields more realistic features of the Kuroshio transport as compared with the authors' previous study, which neglected the vertical heat flux.

1. Introduction

The aim of this manuscript is to suggest a method for estimating the terms of the heat transport of the upper ocean from sequential observations of temperature at sea surface and vertical temperature profiles. These terms are horizontal diffusivity, horizontal velocity, vertical entrainment velocity, the ocean–atmosphere feedback parameter, and the atmospheric forcing correlation time. Our approach is applied to the midlatitude sea surface temperature (SST) anomalies (deviations from the long-term means), having timescales longer than few weeks and shorter than two years. These anomalies can be modeled as a response of the upper ocean to stochastic forcing by synoptic atmospheric events (Hasselmann 1976; Frankignoul and Hasselmann 1977; Reynolds 1978; Frankignoul and Reynolds 1983; Frankignoul 1985; Ostrovskii and Piterbarg 1985, 1995; Piterbarg 1989) since the oceanic upper layer tends to integrate effects of short-term fluctuations in air–sea heat flux, wind-driven mixing, and Ekman pumping and transport (for review see Frankignoul 1985; Piterbarg and Ostrovskii 1997) resulting in timescales of the oceanic thermal response being substantially longer than the limited periods of strong weather forcing. Comparative analysis of the air–sea interactions in different seasons shows that the atmosphere generally drives the midlatitude SST anomaly in the winter season (Cayan 1992).

Recently, Alexander and Deser (1995) drew attention to the importance of vertical entrainment for the evolution of temperature anomalies in the upper ocean. They examined a hypothesis originally proposed by Namias and Born (1970, 1974) and later supported by observation of White and Walker (1974) that sea temperature anomalies created by wintertime mixed layer deepening could be preserved in deeper thermocline waters

Corresponding author address: Dr. Alexander G. Ostrovski, Frontier Observational Research System for Global Change, SEAVANS N. 7th Floor, 1-2-1 Shibaura, Minato-ku, Tokyo 105-6791, Japan.
E-mail: ostrovsk@frontier.esto.or.jp

and the surface in the following fall or winter. Alexander and Deser examined variations in temperature associated with the seasonal cycle observed at ocean weather stations in the North Atlantic and the North Pacific and in the one-dimensional model simulations. Both the data and the model indicated that the Namias–Born mechanism of anomaly reemergence may play an important role in the evolution of the SST. Alexander and Deser stressed the importance of further examining this entrainment in the presence of other processes such as strong horizontal heat transport associated with mean currents and eddies. Below we will estimate these effects in a model of the upper mixed layer heat anomaly balance that includes entrainment, advection, diffusion, feedback, and forcing.

Our model is an extension of the 2D models by Frankignoul and Reynolds (1983), Herterich and Hasselmann (1987), and Ostrovskii and Piterbarg (1985, 1995). Vertical heat flux at the bottom of the upper ocean mixed layer during mixed layer deepening is now included in our model.

This model is fitted to winter temperature data in the North Pacific Ocean in order to obtain vertical entrainment velocity, horizontal diffusivity and advection velocity, feedback factor, and atmospheric forcing parameter. Solving our model inversion consists of three steps: 1) rigorous derivation of a filter (estimator) from the heat conservation equation, 2) data filtration (estimation), and 3) calculation of physical parameters from estimates of the filter coefficients (weights of the estimator).

During the course of this study two problems of rather broad interest are encountered. One problem is due to a need to work with the temperature anomalies, which are essentially the averages in time and space, for example, 10-day anomalies over 1° latitude $\times$ 2° longitude geographical boxes as in this study. We rigorously derive an equation for the average anomalies encompassing all heat transport processes. For example, we will show that the heat advection is not merely a result of the mean currents but, in fact, consists of the two main parts: 1) all motions with scales exceeding the given averaging scales and 2) motion due to the joint effect of fluctuations in the feedback factor and the current velocity. Likewise, we will describe the entrainment, diffusion, feedback, and source terms. The second problem is due to our interest in data averaged over timescales shorter than 1 month. If we are concerned with monthly anomalies, then a ''white noise'' approximation of atmospheric forcing would be worthwhile (Hasselmann 1976). Here, however, we employ higher resolution in time to analyze finer details of the heat transport. We choose to analyze 10-day averaged data. Ten days is close to the period at which the atmospheric forcing spectrum becomes ''color noise''-like in the frequency domain. Thus, a priori, we do not consider the atmospheric forcing as a white noise process and instead assume that the forcing is correlated in time.

This manuscript is organized as follows. In section 2 we propose the heat anomaly balance model and the inversion technique. The derivation of the heat balance equation for the temperature anomalies, averaged both in time and space, and the upper ocean response to a color noise forcing is discussed. The data is introduced in section 3. Section 4 displays the results of the inversion by showing how the SST anomalies are transported in certain regions of the North Pacific Ocean in winter. Section 5 summarizes our findings.

2. Model and inversion technique

Our approach to modeling the SST anomaly variability is based on a hypothesis of timescale separation in the ocean–atmosphere system (Hasselmann 1976). According to this hypothesis, a state of the climate system is defined by a set of fields that can be divided into two parts: the rapidly changing variables basically attributed to weather forcing and the slowly changing variables partly associated with oceanic phenomena. Such a separation leads to statistical closure and, consequently, to statistical reduction of a coupled ocean–atmosphere system. In the resulting model, the oceanic component involves stochastic excitation determined by the second moments of atmospheric input and a feedback from ocean to atmosphere. The corresponding one-dimensional model for the heat anomaly balance of the upper ocean mixed layer accounts for at least 50% of the observed monthly SST anomaly variability throughout the midlatitudes (Reynolds 1978).

The local model of Frankignoul and Hasselmann (1977) and Reynolds (1978) had been extended by Frankignoul and Reynolds (1983), Ostrovskii and Piterbarg (1985), and Herterich and Hasselmann (1987) by including effects of the horizontal advection and diffusion. An autoregressive estimator for the horizontal advection velocities, diffusion coefficients, and the feedback factors from time series of the monthly SST anomalies (Ostrovskii and Piterbarg 1985) was derived. This estimator and the spectrum fitting technique (Herterich and Hasselmann 1987) were independently applied to the SST anomaly data in the North Pacific. Although the spectrum fitting technique yielded a statistically significant velocity estimate, an uncertainty of its diffusivity estimate was found to be of the same order as the estimate itself, so the authors regarded their result only as an order of magnitude estimate. As for the autoregression estimate of the diffusivity, it was thought to be accurate enough if the square root of the product of the diffusion coefficient and the time step, $(D\Delta t)^{1/2}$, is twice as small as the grid step Δl and, in turn, the grid step is at least four times smaller than the spatial scale of the SST anomalies.

Recently, we showed that the autoregression filter can be generalized to involve the case of correlated atmospheric forcing, which can be approximated by a Markov process; that is, the atmospheric spectra are regarded as

color noise–like in the frequency domain instead of being constrained by the white noise approximation as in the original Hasselmann's model. This allowed us to apply the autoregression filter to the time series with averaging interval shorter than 1 month and to improve the time–space resolution of the velocity estimates (Ostrovskii and Piterbarg 1995). More recently this approach was used for inversion of the SST and air–sea heat flux time series for the oceanic near-surface heat anomaly transport, feedback factor, and atmospheric forcing parameter throughout the midlatitude North Pacific (Piterbarg and Ostrovskii 1997).

The autoregression estimator has been intensively tested against the maximum likelihood estimator (Ostrovskii and Piterbarg 1997). The later is a statistical counterpart of the traditional Galerkin method of the computational fluid dynamics. It can generate inversion of high accuracy with relatively few terms in the approximation if the exact solution is sufficiently smooth. The former estimator, which is a statistical analogue of the finite difference model, has the merit of being rigorous since it is derived from the conservation equation instead of substituting finite differences for the partial derivatives. The important advantage of the autoregression filter is that it does not necessarily require the forcing data. For the comparison of these two estimators we took the data simulated in the forward solution of the tracer conservation equation by the Galerkin type method because the Galerkin approach permits approximate solutions of high accuracy, hence providing a general framework for comparing different approximate methods. The tests showed that both methods performed rather well at the time–space grids corresponding to the typical scales of the heat anomaly variability as in the present study though the maximum likelihood estimator feasibility was slightly higher. It should be stressed, however, that the maximum likelihood estimator cannot be immediately applied for verifying the 3D heat balance of the upper ocean because this estimator requires either statistic homogeneity of the transport or a priori knowledge of the temperature spatial modes. The assumption of homogeneity is unsuitable for the vertical processes in the stratified upper ocean and the vertical modes of the temperature variability are hardly known.

Here, we further extend our technique (Ostrovskii and Piterbarg 1995) by incorporating the vertical heat flux into the regression model of the upper-ocean mixed layer heat balance. The mixed-layer heat conservation equation involves conventional parameterization of the vertical heat flux via entrainment during the upper mixed layer deepening. Overall, unlike the previous inversions, which are concerned only with the air–sea heat exchange and the horizontal heat transport, here we consider a closed heat balance of the upper ocean mixed layer.

a. A statistical model for the anomalous heat balance

Let $T'(t, \mathbf{r})$, $\mathbf{r} = (x, y)$ be a field of the SST anomalies; that is, $T' = T - \overline{T}$ is the difference between the current temperature and the annual cycle. For some prescribed time and horizontal scales, τ, L_x, L_y (say, 10 days, 2° longitude, and 1° latitude as in this study), let us denote by $\langle T'(t, \mathbf{r})\rangle$ the average of $T'(t, \mathbf{r})$ in the rectangle centered at $\mathbf{r}$ with sides of length L_x and L_y, and over the time interval τ centered at t. It is important to stress that $\langle T'\rangle$ is a fluctuation with respect to the annual cycle and is a mean with respect to processes having scales less than τ, L_x, L_y. To justify our statistical model, a closed equation for $\langle T'(t, \mathbf{r})\rangle$ is derived from the heat balance equation governing the original temperature field $T(t, \mathbf{r})$. The advection–diffusion equation for the upper-ocean mixed layer heat balance averaged over small time and space scales, say, 1 day and 1 km is (see, e.g., Frankignoul 1985):

$$\frac{\partial T}{\partial t} + \mathbf{u}\cdot\boldsymbol{\nabla}T - \kappa\nabla^2 T = -\frac{w_e}{h}(T - T_h) - \lambda_a T + E, \quad (1)$$

where $T = T(t, \mathbf{r})$ is the temperature of the upper ocean mixed layer of depth h at time t and location $\mathbf{r}$, $T_h = T_h(t, \mathbf{r})$ is the temperature below the upper ocean mixed layer, w_e is the vertical entrainment velocity $w_e = \partial h/\partial t$ when $\partial h/\partial t > 0$ and $w_e = 0$ otherwise, $\mathbf{u}$ is the horizontal velocity, κ is the coefficient for small-scale horizontal diffusion processes, and λ_a is the feedback factor. The right-hand side of (1) represents the heat fluxes in and out of the mixed layer from below (first term) and above,

$$Q/(\rho_w C_{pw} h) = E - \lambda_a T. \quad (2)$$

Equation (2) is a linearization of the air–sea heat flux Q with respect to the sea temperature and h is the mixed layer depth. Let us denote

$$\lambda_e = \frac{w_e}{h}. \quad (3)$$

Note that so far $\mathbf{u} = \mathbf{u}(t, \mathbf{r})$, $\lambda_a = \lambda_a(t, \mathbf{r})$, $\lambda_e = \lambda_e(t, \mathbf{r})$ and $E = E(t, \mathbf{r})$ are stochastic fields with periods longer than 1 day and space scales larger than 1 km.

The traditional closing problem for $\langle T'\rangle$ is essentially complicated in our case by two facts. First, we have to assume that the random fields $\mathbf{u}$, λ_a, λ_e, and E are correlated because their stochastic variability is mostly due to the same factor: the wind fluctuations. Second, the temperature field considered is a mean and a deviation at the same time depending on the scale of interest.

The procedure given in appendix A results in the following equation for the averaged sea temperature anomalies,

$$\frac{\partial\langle T'\rangle}{\partial t} + \mathbf{u}_{\text{net}}\cdot\boldsymbol{\nabla}\langle T'\rangle - \boldsymbol{\nabla}\cdot\mathbf{D}\boldsymbol{\nabla}\langle T'\rangle = -\lambda_{e,\text{net}}\langle T' - T'_h\rangle - \lambda_{a,\text{net}}\langle T'\rangle + S_{\text{net}}, \quad (4)$$

where the net advection velocity, feedback factors, diffusivity and net forcing are given by

$$\mathbf{u}_{\text{net}} = \mathbf{u}_{\text{net}}(t,\mathbf{r}) = \langle \mathbf{u} \rangle - \int_{-\tau_E}^{\tau_E} \langle \mathbf{u}''(0,\mathbf{r})\lambda''(s,\mathbf{r}) \rangle \, ds, \tag{5}$$

$$\lambda_{a,\text{net}} = \lambda_{a,\text{net}}(t,\mathbf{r}) = \langle \lambda_a \rangle + \langle \lambda_e - \overline{\lambda}_e \rangle - \frac{1}{2}\left[\int_{-\tau_E}^{\tau_E} (\langle \boldsymbol{\nabla}\mathbf{u}''(0,\mathbf{r})\lambda''(s,\mathbf{r}) \rangle + \langle \lambda''(0,\mathbf{r})\lambda''(s,\mathbf{r}) \rangle) \, ds \right], \tag{6}$$

$$\lambda_{e,\text{net}} = \overline{w_e/h}, \tag{7}$$

$$\mathbf{D} = \mathbf{D}(\mathbf{r}) = \frac{1}{2} \int_{-\tau_E}^{\tau_E} \langle \mathbf{u}''(0,\mathbf{r})\mathbf{u}''(s,\mathbf{r})^{\mathrm{T}} \rangle \, ds, \tag{8}$$

$$S_{\text{net}} = S_{\text{net}}(t,\mathbf{r}) = \langle S' \rangle - \frac{1}{2}\left(\int_{-\tau_E}^{\tau_E} (\langle \lambda''(0,\mathbf{r})S''(s,\mathbf{r}) \rangle + \langle \mathbf{u}''(0,\mathbf{r}) \cdot \boldsymbol{\nabla} S''(s,\mathbf{r}) \rangle) \, ds \right), \tag{9}$$

$$S' = -\lambda_e'(\overline{T} - \overline{T}_h) + \overline{\lambda_e'(T' - T_h')} - \lambda_a'\overline{T} + \overline{\lambda_a' T'} + E' - \mathbf{u}' \cdot \boldsymbol{\nabla}\overline{T} + \overline{\mathbf{u}' \cdot \boldsymbol{\nabla} T'}. \tag{10}$$

Here the overbar means a conventional Reynolds averaging applied to the annual cycle and anomalies (see appendix A). The double primes denote the departure from the mean defined by the angle brackets, $\lambda'' = \lambda_a'' + \lambda_e''$, τ_E is a common (Eulerian) time correlation scale for the double primed variables. It is assumed that τ_E is small (scale separation). For details about this approximation see Piterbarg and Ostrovskii (1997, p. 228). Notice the small-scale diffusion was neglected in the expression for the effective diffusivity.

It is natural to introduce

$$w_{e,\text{net}} = \lambda_{e,\text{net}}\overline{h}. \tag{11}$$

Simple probabilistic reasonings given in appendix B show that under wide conditions

$$w_{e,\text{net}} > \overline{w}_e. \tag{12}$$

The value of the ratio $w_{e,\text{net}}/\overline{w}_e$ depends on the probabilistic distribution of h', which is unfortunately unknown. However, we can find this ratio from the data. Indeed, the left-hand side of (12) is estimated from our inversion method, while the right-hand side can be directly computed from the series of h. It is interesting that this ratio turns out to be really greater than 1 in accordance with (12), thereby indirectly supporting the model (4).

We underscore that the obtained relations (5)–(10) are not intended for any accurate quantitative estimates. Moreover, they cannot be used for this aim because of the restrictive assumptions (Gaussianity, scale separation) and the noncomputable correlations they include. Instead we set up to estimate $\mathbf{u}_{\text{net}}$, D, $\lambda_{a,\text{net}}$, and $w_{e,\text{net}}$ from the observations of $\langle T' \rangle$, $\langle T_h' \rangle$, and climate fields of $\overline{h}$ under the assumption that the right-hand side (source) of (4) is a random field, while $\mathbf{u}_{\text{net}}$, D, $\lambda_{a,\text{net}}$, and $w_{e,\text{net}}$ are deterministic parameters changing slowly in space while remaining constant during a season. Definitely, one can view (4) as a phenomenological model for an anomalous heat balance in the upper ocean and at once proceed to its inversion with respect to the unknown parameters. There is no doubt that even such a straightforward approach would give a lot of information about the heat anomaly variability. However, we prefer to derive, eventhough approximately, (4) from (1) in order, first, to lay a physical ground for the statistical model and, second, to show that the net advection and the net atmosphere–ocean feedback parameter are distorted by subgrid processes. Yet, it is important to note that the diffusivity and the entrainment keep the original physical meaning. Notice, that the net source includes the generation of SST anomalies due to the forcing of the mean SST field by the fluctuating currents and heat fluxes. This forcing can be primarily attributed to the wind stress variations leading to anomalous Ekman currents and heat flux anomalies. The SST anomaly generation by the second, fourth, and seventh terms in the expression (10) for S' varies with season. This seasonal effect can be basically addressed when we fit the statistical model to the data for only one season, particularly the cool season.

b. Regression model for the upper ocean temperature

A regression model for discrete temperature observations based on the stochastic equation (4) is now derived. In fact, our model is a hybrid autoregression–regression model since the resulting equations connect the value of the SST anomaly at a fixed point $\mathbf{r}_0$ of a prescribed grid at moment n with 1) the SST anomalies at moment $n - 1$ at this and neighbor points (autoregression) and 2) with the temperature anomaly at the bottom of the upper ocean mixed layer at the same point $\mathbf{r}$ at moment $n - 1$ (regression). Thus, the later temperature anomaly is included as a regressor. First, for the sake of clarity, change notation in (4) by dropping all subscripts and angle brackets; that is, set

$$T = \langle T' \rangle, \qquad T_h = \langle T_h' \rangle.$$

Then assume an isotropic diffusivity and rewrite the equation as follows:

$$\frac{\partial T}{\partial t} + \mathbf{u} \cdot \boldsymbol{\nabla} T - D\nabla^2 T + \lambda T = \lambda_e T_h + S(t,\mathbf{r}), \tag{13}$$

where

$$\lambda = \lambda_a + \lambda_e. \tag{14}$$

Let Δt, Δx, Δy be prescribed time and space steps

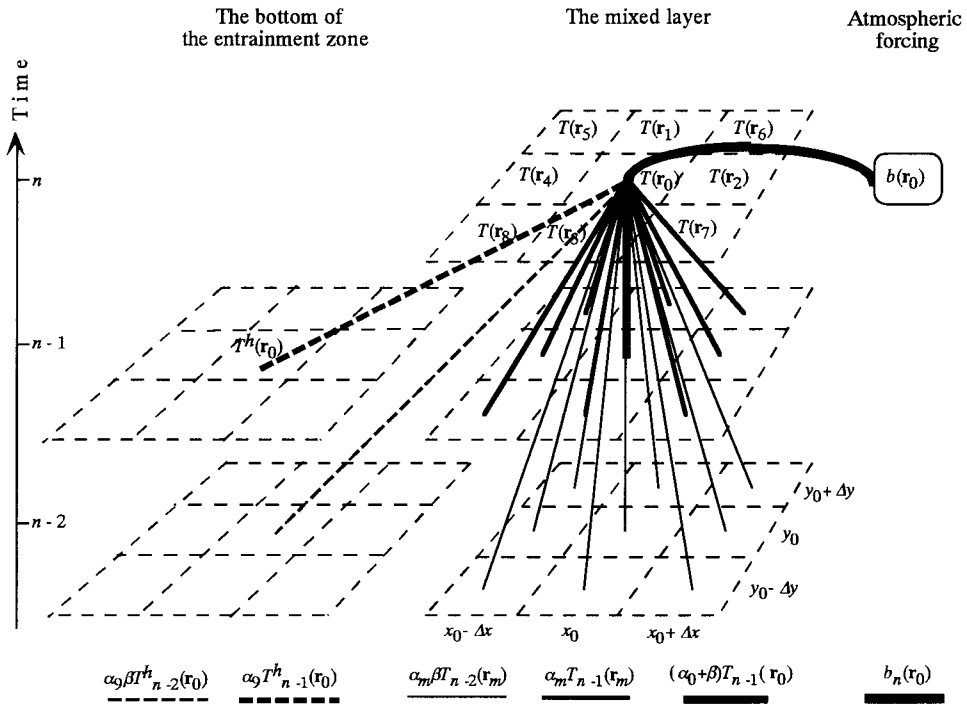

FIG. 1. The spatiotemporal links in the regression model. The SST anomaly at time $n\Delta t$ in grid box $\mathbf{r}_0$ depends on the SST anomalies at two previous time steps in the surrounding boxes. It also depends locally on the atmospheric forcing and the previous temperature anomalies below the mixed layer.

and $\mathbf{r}_0 = (x_0, y_0)$ be a fixed point of the grid $\{i\Delta x, j\Delta y, i, j = 0, 1, 2, \cdots\}$. Denote

$$T_n(\mathbf{r}) = T(n\Delta t, \mathbf{r}), \qquad T_n^h(\mathbf{r}) = T_h(n\Delta t, \mathbf{r}). \quad (15)$$

In appendix C we show that

$$T_n(\mathbf{r}_0) = \sum_{m=0}^{8} \alpha_m T_{n-1}(\mathbf{r}_m) + \alpha_9 T_{n-1}^h(\mathbf{r}_0) + \varepsilon_n(\mathbf{r}_0), \quad (16)$$

where α_m are coefficients. The neighboring grid points are defined as follows: $\mathbf{r}_1 = (x_0, y_0 + \Delta y)$, $\mathbf{r}_2 = (x_0 + \Delta x, y_0)$, $\mathbf{r}_3 = (x_0, y_0 - \Delta y)$, $\mathbf{r}_4 = (x_0 - \Delta x, y_0)$, $\mathbf{r}_5 = (x_0 - \Delta x, y_0 + \Delta y)$, $\mathbf{r}_6 = (x_0 + \Delta x, y_0 + \Delta y)$, $\mathbf{r}_7 = (x_0 + \Delta x, y_0 - \Delta y)$, $\mathbf{r}_8 = (x_0 - \Delta x, y_0 - \Delta y)$. The noise is given by the first-order Markov process:

$$\varepsilon_n(\mathbf{r}) = \beta\varepsilon_{n-1}(\mathbf{r}) + b_n(\mathbf{r}), \quad (17)$$

where β is an autoregression coefficient, and $b_n(\mathbf{r})$ is a white noise in time.

The regression coefficients α_m are related to the unknowns u, v, w_e, D, λ, and β by formulas (C8) from appendix C (u and v are the zonal and meridional components of the velocity).

Substituting (17) into (16) we obtain the following form of the regression model for the random fields of the sea surface temperature, the temperature at the bottom of the upper mixed layer, and the colored noise forcing by the atmosphere over the discrete time–space grid:

$$T_n(\mathbf{r}_0) = \sum_{m=0}^{8} \alpha_m[T_{n-1}(\mathbf{r}_m) - \beta T_{n-2}(\mathbf{r}_m)] + \alpha_9[T_{n-1}^h(\mathbf{r}_0) - \beta T_{n-2}^h(\mathbf{r}_0)] + \beta T_{n-1}(\mathbf{r}_0) + b_n(\mathbf{r}_0). \quad (18)$$

Thus, the model (18) sets up the spatiotemporal links between the time series $T_n(\mathbf{r})$, $T_n^h(\mathbf{r})$, and $b_n(\mathbf{r})$ as shown in Fig. 1. The SST anomaly $T_n(\mathbf{r}_0)$ at time step n in box $\mathbf{r}_0$ is related to the temperature anomalies of the previous time steps $n - 1$ and $n - 2$ at the same box and eight neighboring boxes: a link to the preceding SST anomaly $T_{n-1}(\mathbf{r}_m)$ is measured by the weight (coefficient) α_m and a link to the earlier anomaly $T_{n-2}(\mathbf{r}_m)$ by the weight $\alpha_m\beta$. The relations among the present SST anomaly, $T_n(\mathbf{r}_0)$, and two recent temperature anomalies at the bottom of the entrainment zone, $T_{n-1}^h(\mathbf{r}_m)$ and $T_{n-2}^h(\mathbf{r}_m)$, are defined locally by the weights α_g and $\alpha_g\beta$, respectively. Noticeably, the local atmospheric forcing effect is split into two parts: one part results in internal links with duration of $2\Delta t$ in the temperature anomaly fields and the other represents the contemporary contribution $b_n(\mathbf{r}_0)$. While the coefficients α_m are basically responsible for short memory (10 days in this study), the products of the coefficients α_m and β are responsible for prolonged memory (20 days in this study). The coefficient β measures the difference between the color noise and white noise approximations of the forcing term. The

value $\beta = 0$ indicates that the color noise approximation yields no improvement over the white noise one.

The estimation of $\alpha_0, \alpha_1, \ldots, \alpha_g$, and β is based on the least squares method. Namely, after multiplying (18) by $T_n(\mathbf{r}_l)$, $l = 0, 1, \cdots, 8$ and averaging through time, we arrive at the following system of nine simultaneous equations:

$$\gamma_1^{0l} - \sum_{m=0}^{9} \alpha_m(\gamma_0^{lm} - \beta\gamma_1^{lm}) + \beta\gamma_0^{0l} = 0, \quad (19)$$

where

$$\gamma_s^{ij} = \langle T_n(\mathbf{r}_i)T_{n-s}(\mathbf{r}_j)\rangle \quad (20)$$

is the covariance between the time series $T_n(\mathbf{r}_i)$ and $T_{n-s}(\mathbf{r}_j)$ with a time lag $s = 0, 1, 2$ in 10-day intervals; now $T_n(\mathbf{r}_9)$ stands for $T_n^h(\mathbf{r}_0)$. Notice that the covariance

$$\langle T_{n-s}(\mathbf{r}_i)b_n(\mathbf{r}_j)\rangle = 0, \qquad s \geq 1 \quad (21)$$

because $\{b_n(\mathbf{r})\}$ is white noise in time.

The regression model (18) can be fitted to seasonally sampled data allowing us to retain the seasonal features of the air–sea interactions. This is important because the Hasselmann approach is most appropriate in winter when the atmosphere drives the midlatitude SST variability (Cayan 1992). While the SST anomalies $T_n(\mathbf{r})$ are departures from the 10-day norms varying with the annual cycle, we can evaluate their covariances at matched seasonal period; for example in winter as in the present study, by the following formula

$$\gamma_s^{ij} = \frac{1}{(M-1)N}\sum_{d=2}^{M}\sum_{k=1}^{N} T_{d+36k}(\mathbf{r}_i)T_{d-s+36k}(\mathbf{r}_j) - \frac{1}{(M-1)^2N^2}\sum_{d=2}^{M}\sum_{k=1}^{N} T_{d+36k}(\mathbf{r}_i)\sum_{d=2}^{M}\sum_{k=1}^{N} T_{d+36k}(\mathbf{r}_j), \quad (22)$$

where M is the number of 10-day intervals in the matched season and N is the total number of observational years. The value γ_s^{ij} represents the covariance of the available overlapped portions of the time series.

To estimate the vertical entrainment velocity w_e, the horizontal advection velocities u and v, the diffusion coefficient D, the feedback factor λ_a, and the atmospheric forcing parameter β we substitute expressions (C8) for α_m into (19) and solve the new nonlinear system numerically. In our previous studies (Ostrovskii and Piterbarg 1995; Piterbarg and Ostrovskii 1997) we divided the area into overlapped sets of grid boxes and searched for the solutions of the inverse problems in the individual sets of the grid boxes. Here, instead, we solve a single inversion problem for the entire observational domain.

The resulting system (19) defined over the observational grid is overdetermined with respect to the unknowns w_e, u, v, D, λ_a, β. One possibility to avoid uncertainty in the solution is to constrain the problem by the divergence norm

$$\frac{\partial h}{\partial t} + \frac{\partial(hu)}{\partial x} + \frac{\partial(hv)}{\partial y} = 0. \quad (23)$$

Such a constraint is common for treating uncertainties in tracer inversions. For example, Kelly (1989) and Kelly and Strub (1992) applied it to get more realistic near-surface ocean current velocity fields in the inversion of satellite infrared images. Other constraints such as the kinetic energy norm and the relative vorticity norm could be introduced in the inversion, too (see Kelly 1989). Here, we do not use constraints other than (23) because in the heat anomaly balance equation we have the net advection velocity rather than the current velocity.

Thus, we do not solve the problem explicitly but obtain the vector $\mathbf{Q} = (w_e, u, v, D, \lambda_a, \beta)$, which gives a local minimum for the sum of squares

$$S(\mathbf{Q}) = F_1(\mathbf{Q})^2 + \cdots + F_{10}(\mathbf{Q})^2, \quad (24)$$

where $F_1, \ldots, F_9$ are the functions on the left-hand side of (19) and F_{10} is the function on the left-hand side of (23).

The inversion employs the Levenberg–Marquardt–Morrison method (Scientific Subroutine Library 1987). The search for the solution starts from different initial vectors $\mathbf{Q}_{\text{initial}}$ and the solution is chosen to be that vector $\mathbf{Q}_{\text{final}}$, which provides the smallest value of $S(\mathbf{Q})$. The quantity $S(\mathbf{Q})$ is minimized iteratively until a predetermined convergence criteria is satisfied. The convergence criteria should be small enough to provide us with the misfits less than several percent of the values of the observed covariances γ_1^{0l} (e.g., Ostrovskii and Piterbarg 1997).

3. Data

We use the temperature data from the Comprehensive Ocean–Atmosphere Data Set Compressed Marine Reports for the sea surface and the World Ocean Atlas 1994 Profile Data Set at standard depth levels. The North Pacific row data are averaged over 1° latitude × 2° longitude boxes from 10° to 60°N for sequential 10-day intervals during 1965–90. A grid size on the order of 100 km basically exceeds the typical scale of ocean synoptic process such as rings and eddies. Therefore, with respect to parameterizing subgrid processes, our estimates of the diffusion coefficients mainly represent mesoscale diffusivity. The averaged data are compiled only for the winter season, that is, from the last 10-day period of November until the end of March, when the SST anomaly field is forced by the air–sea heat flux (Cayan 1992). To obtain the anomalies, the long-term 10-day norms were subtracted from the time series. The upper-ocean mixed layer depths were derived by conventional criteria of the potential density gradient from the 10-day vertical profiles, allowing us to retrieve the time series of the temperature anomalies below the

mixed layer. Then the long-term 10-day norms of the average cycle of the mixed layer depths were computed.

We use only those time series that could provide at least 30 samples for calculation of the covariances (20). As a result, there is only enough data in two regions: 1) along the western boundary of the Pacific basin east of the Honshu, Kyushu, and Okinawa Islands and 2) between the California coast and the Hawaiian Islands. The significance of the covariance estimates γ_s^{ij} at each i, j, and s was improved by a spatial smoothing with a 3×3 boxcar kernel. The sense of this smoothing is similar to that of smoothing over an ensemble of estimates that is conventional for making the spectral estimates consistent (Bendat and Piersol 1971). The smoothing of the covariance estimates results in growth of spatial coherence in the SST anomaly propagation that is in contrast to smoothing of the original data, which could result in eliminating information on the directional transport.

4. Estimates of the heat anomaly transport

A novelty of this study is primarily due to incorporating the entrainment effect into the heat anomaly transport model used for inversion of the upper ocean temperature data. As was shown in section 2, estimate for the entrainment velocity w_e is not an estimate of the average, which might be inferred from the mean deepening of the mixed layer, but includes the contributions associated with the daily scale processes, which we do not measure very well. This inversion allows us to make more complete assessment of the heat flux due to entrainment in terms of the rate of the mixed layer deepening.

Figure 2 demonstrates distribution of the net entrainment velocity in the two observational domains near the ocean western boundary and in the region between the California coast and the Hawaiian islands. The entrainment velocities are found to be of the order of 10^{-5} m s^{-1}. This estimate is slightly higher than the average deepening of the upper mixed layer. For example, at Ocean Weather Station N (30°N, 140°W) the mixed layer usually deepens from 75 m in November to 130 m in March (e.g., Alexander and Deser 1995) while our estimate of the net entrainment velocity is nearly 1 m day^{-1} for this location. This suggests that in terms of the rate of the mixed layer deepening, the contribution associated with events having the daily timescale could be of the same order as that measured by the long-term average increase in the mixed layer depth during winter.

It is noteworthy that the entrainment is enhanced in the vicinity of strong currents. Such an intensification occurs near North Equatorial Current and in the Kuroshio–Oyashio frontal zone. The entrainment is particularly significant east of Honshu and south of Kyushu that is, along the Kuroshio where the estimates of w_e can reach a few meters per day. More intensive entrainment can be associated with the vertical shear velocity at the bottom of the mixed layer. The entrainment can be partly maintained by transfer of kinetic energy from the mean flow into turbulence as a result of friction at the bottom of the mixed layer (Lofquist 1960; Csanady 1978).

Taking into account the entrainment effect allows us to obtain more realistic departures of the Kuroshio and Oyashio currents from the western boundary as compared with the previous study (Ostrovskii and Piterbarg 1995). Figure 3a shows the net advection velocities near the western boundary of the North Pacific Ocean. The Kuroshio transport is evident south of Kyushu where its speed is about 0.15–0.4 m s^{-1}. This transport separates from the coast at 33°–34°N and flows eastward. The strong eastward flow and the correct latitude of separation are major gains as compared with the previous inversions that neglected the entrainment effect. However the grid resolution does not allow estimation of the northward Kuroshio flow along the island of Okinawa.

The other features of the net advection field consistent with observations of the ocean near-surface currents are as follows. The first one is an indication of the Kuroshio meandering southeast of Kyushu (see Imawaki et al. 1996). The second is a large quasi-stationary meander at 144°E (Yasuda et al. 1992; Ichikawa and Imawaki 1994) and associated local recirculation. The third feature is an indication of the intensification of the eastward flow near the Subarctic Front and relatively weak flow between the Kuroshio Extension and the Subarctic Front jet, which agrees well with recent findings from drifter tracks (Maximenko et al. 1999). Finally, in the subtropical gyre, except at 15°N, there is a broad westward flow of up to 0.2 m s^{-1} speed consistent with observations of the North Equatorial Current and the recirculation of the Kuroshio (e.g., Nitani 1972; Hasunuma and Yoshida 1978, among others).

The overall advection velocity pattern in the northeast Pacific (Fig. 3b) is in agreement with our previous results (Piterbarg and Ostrovskii 1997). Now, however, the convergence of the advection field is definitely more smooth. The advection is directed eastward from the midlatitude ocean interior at 30°–40°N. This advection with speed of 0.05–0.15 m s^{-1} seems to be associated with the broad North Pacific Current (Sverdrup et al. 1946). The eastward transport eventually vanishes near the subtropical convergence zone.

East and south of the subtropical convergence zone, the westward transport dominates. In the region where the California Current departs from the coast and extends in a west-southwest direction (Batteen et al. 1995), the westward advection velocity is as high as 0.2 m s^{-1}. Other processes such as offshore Ekman drift and Rossby waves (Killworth et al. 1997; Qiu et al. 1997) may also result in the westward transport.

The existence of the heat anomaly convergence has important implications. It explains why the rotated EOF first mode for SST anomalies (Tourre and White 1995)

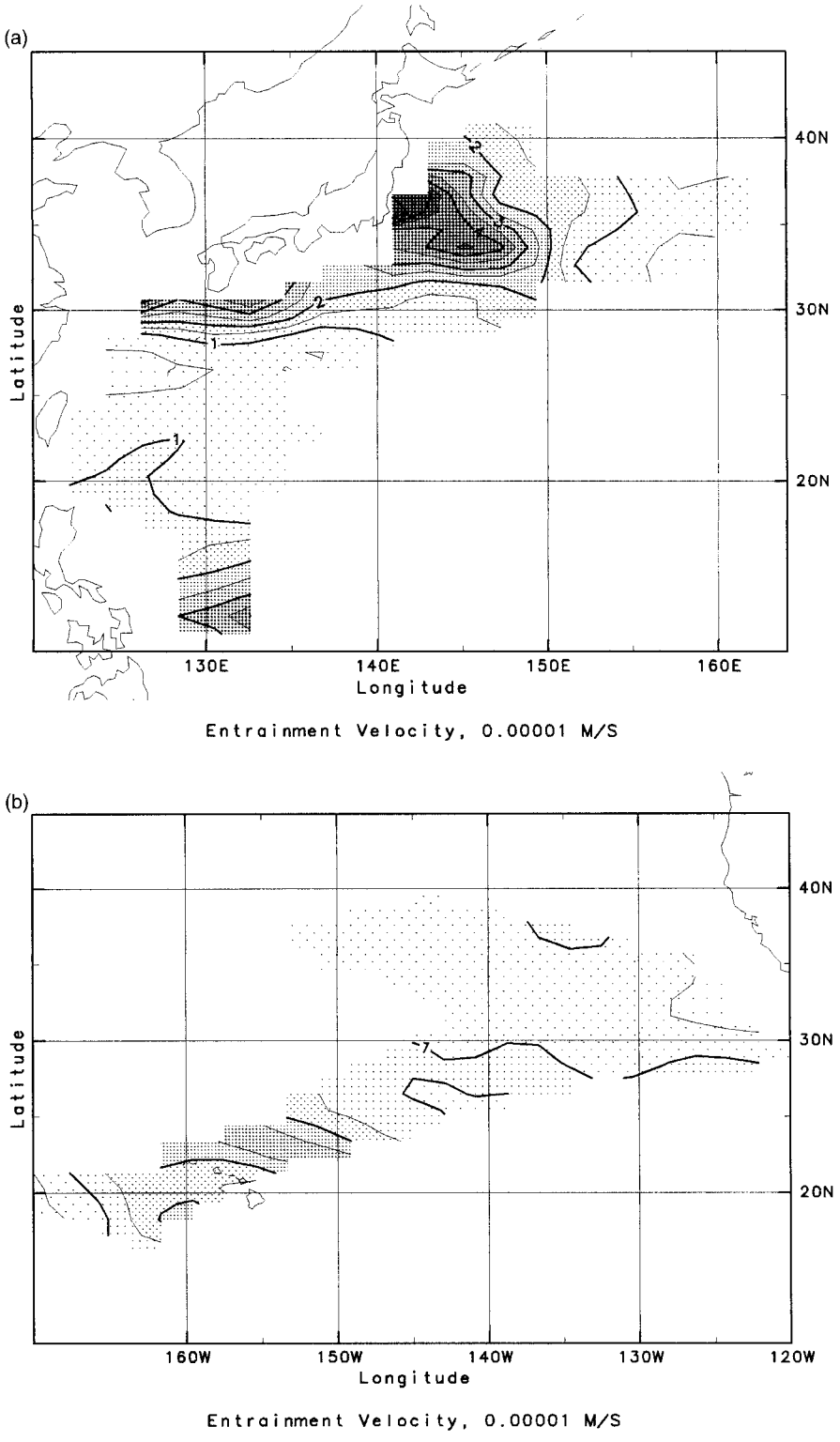

FIG. 2. The distribution of the entrainment velocity w_e (0.000 01 m s^{-1}) in (a) the northwest Pacific and (b) the northeast Pacific.

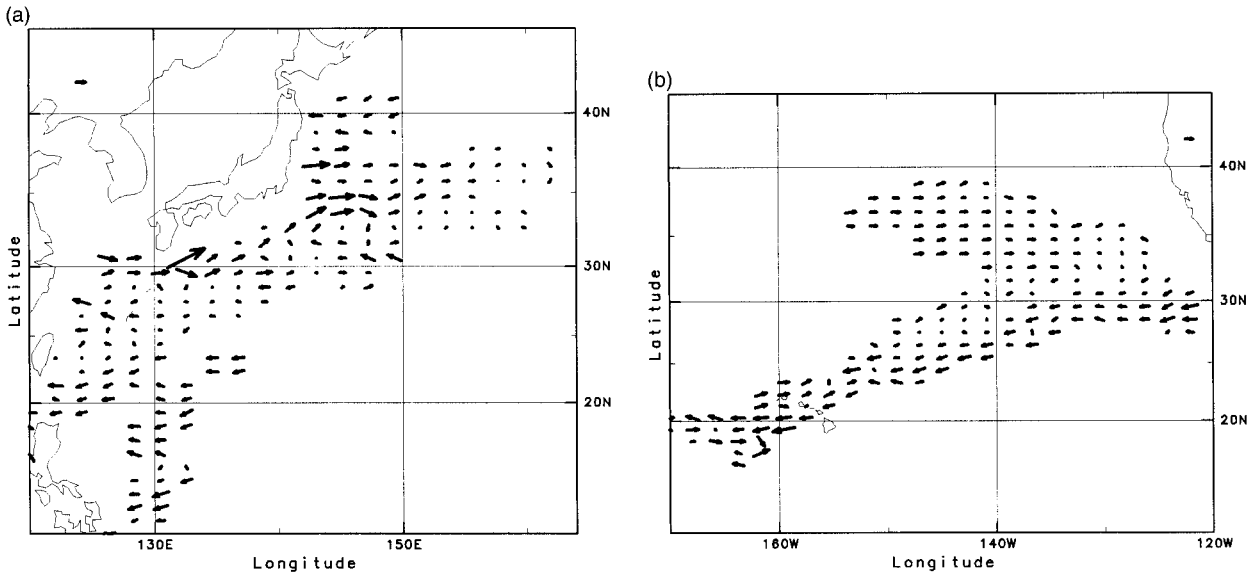

FIG. 3. The distribution of the net advection velocity **u** (m s^{-1}) in (a) the northwest Pacific (an arrow in the upper-left corner indicates velocity of 0.1 m s^{-1}) and (b) the northeast Pacific (an arrow in the upper-right corner indicates velocity of 0.1 m s^{-1}).

shows a distinct boundary between positive and negative loadings that is stretched from California to Hawaii. As follows from Fig. 3b of this manuscript and Fig. 7 of Tourre and White (1995), the SST anomalies of opposite signs are often translated to a convergence where they cancel each other out, thereby resulting in minimum SST anomaly variance.

It should be stressed that these velocity vector estimates do not imply that the anomalies always travel with such an inferred speed in the estimated direction. Rather, they indicate the most probable path and speed while in a number of cases the anomalies may translate in different directions as indicated by visual tracking of their movements.

The smoothness of the advecting field is controlled largely by the divergence norm in the interior of the geographical domain. To obtain more smoothness inside the domain, it is possible to attach weight (more than 1) to the divergence norm or to introduce other a priori smoothness constraints to the net advection. The net advection estimate should be treated with caution at the boundary where smoothness constraints are less adequate.

The estimates of the heat diffusivity are less interesting, showing little variation of the diffusion coefficient over the observational domain: the values of D lie in the range of 4–5 ($\times 10^{-3}$ m^2 s^{-1}) (Fig. 4). Perhaps, more would be learned from the inversion when both latitudinal and zonal diffusivities are sought (e.g., Ostrovskii and Piterbarg 1997) instead of the isotropic horizontal diffusion coefficient as in this study.

The absolute values of the atmospheric forcing parameter estimates (not shown here) are less than 0.2, indicating insignificantly weak relationship between the atmospheric forcing events at time intervals of 10 days, the result that seems to be reasonable for the regions concerned in this study.

5. Conclusions

This study eliminates one shortcoming of the previous inversion studies aimed at obtaining the ocean near-surface heat transport from sequential fields of sea surface temperature. While earlier inversions were concerned only with the horizontal transport, the present estimator also includes the vertical heat flux. Our model is based on a mixed layer conservation equation featuring horizontal advection, Laplacian closure for diffusion processes, conventional parameterization of vertical heat flux due to entrainment during the mixed layer deepening, and a stochastic atmospheric forcing. The model can be viewed as 2D in horizontal and $\frac{1}{2}$D in vertical since it requires information on the temperature at the bottom of the entrainment zone. The inversion is treated as a statistical problem with a stochastic partial differential equation for heat conservation in the upper ocean mixed layer. This approach allows us to derive the regression estimator that results in obtaining the unknowns—the vertical entrainment velocity, the horizontal velocity and diffusivity, the feedback factor, and the atmospheric forcing parameter—from the time series of the sea temperature profiles. In a wider sense, the regression estimator constitutes a solution of the familiar inverse problem of deriving oceanic near-surface dynamics from time-dependent distributions of a tracer in the case when forcing is stochastic. Perhaps, this approach can be applied to other boundary layers in fluids.

The assumption about the stochastic source is advantageous because it allows consideration of the conservation equation for fluctuations from the mean state,

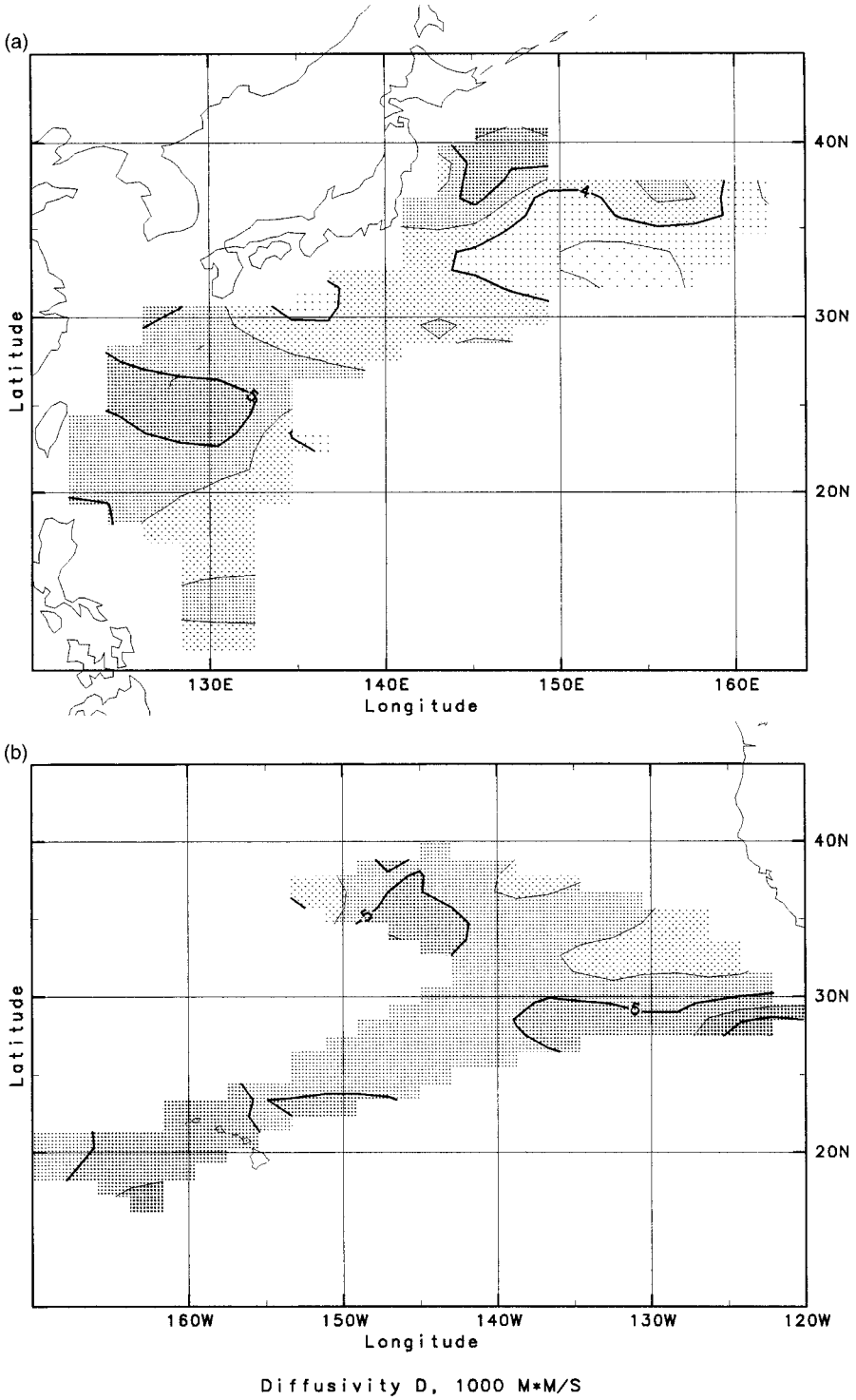

FIG. 4. The distribution of the heat diffusivity D ($m^2\ s^{-1}$) in (a) the northwest Pacific and (b) the northeast Pacific.

which can be easily obtained in most practical applications. Also, introduction of the stochastic term enables more clear definition for the impact of observational noise that otherwise is hard to treat in terms of the finite-difference approximations. As was shown in Piterbarg and Ostrovskii (1997), an increase (decrease) in the source variance due to random observational errors results in enhancement (decline) of the diffusion coeffi-

cients and the feedback factor inferred by the autoregression estimator. Therefore, the effects of the random observational errors are also localized in the estimates of the dissipation terms. In our earlier paper (Ostrovskii and Piterbarg 1995), the entrainment was supposed to be a part of the feedback. In such a formulation, both the entrainment and the diffusivity work for the dissipation. The numerical experiments have suggested that to preserve the dissipation, the diffusion coefficient must be larger if the feedback is smaller (Piterbarg and Ostrovskii 1997). Here, however, the entrainment is formulated explicitly and may lead to recurrence of the SST anomalies due to the Namias–Born mechanism, examined by Alexander and Deser (1995).

This study shows that the stochastic partial differential equation of the heat anomaly balance in the upper ocean can be reduced to a regression estimator, which has distinct physical meaning since its coefficients can be linked to the physical parameters by a rather simple formula. It is encouraging that the autoregression version of this filter has been successfully tested in numerical experiments with a tracer in a broad range of conditions typical for the upper ocean variability (Ostrovskii and Piterbarg 1997). The regression estimator is applicable to the rather general case when atmospheric forcing is not a white noise but instead is a Markov process in time.

The regression filtering of the North Pacific temperature anomaly data results in obtaining the horizontal and vertical heat transport in two regions of the North Pacific: near the Kuroshio and Oyashio and along the subtropical convergence zone in the eastern part of the ocean. The broad agreement of both vertical entrainment velocity and horizontal advection velocity estimates with the known features of the upper ocean dynamics indicate that the proposed estimator captures the essential physics of the heat anomaly balance. By adding the vertical heat flux into the inversion model we succeeded to demonstrate more clearly a role that the Kuroshio and the Subarctic Front jet play in the near-surface heat anomaly transport. The divergence adjustment of the upper mixed layer allows the estimator to assess an indirect effect of the entrainment. It is important that within the framework of our approach, it is possible to define the physical meaning of the estimates derived from the averaged data. For example, the vertical entrainment velocity estimate is not merely a mean rate of the mixed layer deepening, but rather it is a net estimate that also includes the contribution due to short period fluctuations of the mixed layer, which are difficult to measure in situ. Overall, this study improves our ability to extract information on the ocean near-surface dynamics from sequential temperature fields.

Acknowledgments. The support of both the U.S. Office of Naval Research via Grant N00014-99-0042 and the Ministry of Education, Science, and Culture of Japan is acknowledged. We thank Arthur Mariano and the anonymous reviewers for useful comments and remarks that significantly improved the manuscript.

APPENDIX A

Averaging Equation for the SST Anomalies

The derivation (4) from (1) includes three successive steps. The first two are just algebraic and do not require any restrictions; the last one is based on the strong assumptions of Gaussianity and scale separation.

Let each property in (1) be decomposed into a seasonally varying mean (norm) and a departure from the norm (anomaly), for example, $T = \overline{T} + T'$. The first step is a conventional Reynolds averaging applied to the annual cycle and anomalies. It results in a nonclosed equation for the mean temperature field

$$\frac{\partial \overline{T}}{\partial t} + \overline{\mathbf{u}} \cdot \boldsymbol{\nabla} \overline{T} + \overline{\mathbf{u}' \cdot \boldsymbol{\nabla} T'} = \kappa \nabla^2 \overline{T} - \overline{\lambda}_e (\overline{T} - \overline{T}_h) - \overline{\lambda'_e (T' - T'_h)} - \overline{\lambda T} - \overline{\lambda' T'} + \overline{E}. \tag{A1}$$

Subtract (A1) from (1) and keep all terms

$$\frac{\partial T'}{\partial t} + \mathbf{u} \cdot \boldsymbol{\nabla} T' = \kappa \nabla^2 T' - \lambda_e (T' - T'_h) - \lambda_a T' + S', \tag{A2}$$

where the new source term

$$S' = -\lambda'_e (\overline{T} - \overline{T}_h) + \overline{\lambda'_e (T' - T'_h)} - \lambda' \overline{T} + \overline{\lambda' T'} + E' - \mathbf{u}' \cdot \boldsymbol{\nabla} \overline{T} + \overline{\mathbf{u}' \cdot \boldsymbol{\nabla} T'} \tag{A3}$$

includes the generation of SST anomalies due to forcing of the mean SST field. Perhaps, the most important feature of (A2) is that fields $\mathbf{u}$, λ_a, and λ_e are original as in (1). This becomes possible because we do not omit the nonlinear terms during the derivation.

Finally, in the third step, we represent the temperature anomaly and other anomalies as

$$T' = \langle T' \rangle + T'', \tag{A4}$$

where T'' is the departure from the time–space mean, and make the following key assumptions:

- the averaging $\langle \cdot \rangle$ is equivalent to the ensemble averaging;
- $\mathbf{u}''$, λ'', S'' are Gaussian;
- the Eulerian timescale of the subgrid (double primed) processes is much less than other timescales.

Then we apply the averaging procedure given in (Piterbarg and Ostrovskii 1997, chapter 3) to (A2) and arrive at (4).

APPENDIX B

Relation between Net and Entrainment Velocities

Inequality (12) is equivalent to

$$\overline{w_e/h} > \overline{w}_e/\overline{h}. \tag{B1}$$

Assume that fluctuation $h'(t)$ is a stationary Gaussian process in t. Then h' and $w' = \partial h'/\partial t$ taken at the same point are independent; hence, (B1) is equivalent to

$$\overline{1/h} > 1/\overline{h}. \tag{B2}$$

The latter readily follows from Jensen's inequality [see, e.g., Liptser and Shiryayev 1977, p. 18, formula (1.12)].

The ratio in (B2) can be easily found under specific assumptions about the probabilistic distribution of h. For example, assume that h is uniformly distributed in the interval $(h_{\min}, h_{\max})$. Set $\alpha = h_{\max}/h_{\min} > 1$. Then

$$\frac{\overline{1/h}}{1/\overline{h}} = \frac{(\alpha + 1)\ln\alpha}{2(\alpha - 1)}. \tag{B3}$$

One can use this formula for an approximate computation of the ratio of the left- and right-hand sides in (12).

APPENDIX C

Derivation of the Regressor Estimator

Assume in (13) that $S(t, \mathbf{r})$ is a stationary in t random field and $\mathbf{u}$, D, λ_a, and λ_e are constant in time and vary slowly in space in such a way that we can use the Green function for the heat equation with constant coefficients to write down the following approximate solution formula for (13) given an initial condition $T_0(\mathbf{r})$

$$T(t, \mathbf{r}) = \exp(-\lambda(t - t_0)) \int \Phi_{\mathbf{u},D}(t - t_0, \mathbf{r} - \mathbf{r}')T_0(\mathbf{r}')\, d\mathbf{r}' + \exp(-\lambda t) \int_{t_0}^{t} \int \exp(\lambda s)\Phi_{\mathbf{u},D}(t - s, \mathbf{r} - \mathbf{r}')(\lambda_e T_h(s, \mathbf{r}') + S(s, \mathbf{r}'))\, d\mathbf{r}'\, ds, \tag{C1}$$

where the space integration is taken over the whole plane. Here

$$\Phi_{\mathbf{u},D}(t, \mathbf{r}) = \frac{1}{4\pi Dt} \exp\left(-\frac{(\mathbf{r} - t\mathbf{u})^2}{4Dt}\right) \tag{C2}$$

is the Gaussian kernel. The representation (C1) follows from the fact that the Gaussian kernel satisfies the equation

$$\frac{\partial \Phi_{\mathbf{u},D}}{\partial t} + \mathbf{u} \cdot \nabla \Phi_{\mathbf{u},D} = D\nabla^2 \Phi_{\mathbf{u},D} \tag{C3}$$

with the initial condition

$$\Phi_{\mathbf{u},D}(t_0, \mathbf{r}) = \delta(\mathbf{r}), \tag{C4}$$

where $\delta(\mathbf{r})$ is the Dirac delta function.

By substituting $t_0 = (n - 1)\Delta t$, $t = n\Delta t$, and $T_0(\mathbf{r}) = T_{n-1}(\mathbf{r})$ into (C1) and assuming T_h constant through the interval Δt, we get the following recursive equation for any $n = 1, 2, \cdots$

$$T_n(\mathbf{r}) = \nu \int_E \Phi_{\mathbf{u},D}(\Delta t, \mathbf{r} - \mathbf{r}')T_{n-1}(\mathbf{r}')\, d\mathbf{r}' + \frac{w_e(1 - \nu)}{w_e + h\lambda_a} T^h_{n-1}(\mathbf{r}) + \varepsilon_n(\mathbf{r}), \tag{C5}$$

where

$$\nu = \exp(-\lambda\Delta t) \tag{C6}$$

and

$$\varepsilon_n(\mathbf{r}) = \exp(-\lambda n\Delta t) \int_{(n-1)\Delta t}^{n\Delta t} \int_E \exp(\lambda s)\Phi_{\mathbf{u},D}(n\Delta t - s, \mathbf{r} - \mathbf{r}')S(s, \mathbf{r}')\, d\mathbf{r}'\, ds \tag{C7}$$

is a stationary sequence of random fields.

The standard assumption that $S(t, \mathbf{r})$ is a white noise process in t is not valid for the 10-day timescale considered in this study. Instead we assume that the forcing field $\varepsilon_n(\mathbf{r})$ appearing in (C5) depends on the previous values $\varepsilon_{n-1}(\mathbf{r}), \varepsilon_{n-2}(\mathbf{r}), \ldots$. We parameterize this memory in simplest way by assuming the sequence $\{\varepsilon_n(\mathbf{r})\}$ to be a first-order Markov process given by (17). By applying

the procedure of space discretization and interpolation given in (Piterbarg and Ostrovskii 1997, chapter 8) to (C5), we arrive at the regression model (16) with the coefficients related to the unknown parameters by

$$
\begin{aligned}
\alpha_0 &= \nu\left[\frac{5}{9} - \frac{1}{3}\left(\frac{u^2\Delta t}{\Delta x^2} + \frac{v^2\Delta t}{\Delta y^2} + \frac{2D\Delta t}{\Delta x^2} + \frac{2D\Delta t}{\Delta y^2}\right)\right],\\
\alpha_1 &= \nu\left[\frac{2}{9} - \frac{v\Delta t}{6\Delta y} - \frac{1}{3\Delta x^2}(u^2\Delta t^2 + 2D\Delta t) + \frac{1}{6\Delta y^2}(v^2\Delta t^2 + 2D\Delta t)\right],\\
\alpha_2 &= \nu\left[\frac{2}{9} - \frac{u\Delta t}{6\Delta x} - \frac{1}{3\Delta y^2}(v^2\Delta t^2 + 2D\Delta t) + \frac{1}{6\Delta x^2}(u^2\Delta t^2 + 2D\Delta t)\right],\\
\alpha_3 &= \nu\left[\frac{2}{9} + \frac{v\Delta t}{6\Delta y} - \frac{1}{3\Delta x^2}(u^2\Delta t^2 + 2D\Delta t) + \frac{1}{6\Delta y^2}(v^2\Delta t^2 + 2D\Delta t)\right],\\
\alpha_4 &= \nu\left[\frac{2}{9} + \frac{u\Delta t}{6\Delta x} - \frac{1}{3\Delta y^2}(v^2\Delta t^2 + 2D\Delta t) + \frac{1}{6\Delta x^2}(u^2\Delta t^2 + 2D\Delta t)\right],\\
\alpha_5 &= \nu\left[-\frac{1}{9} + \frac{u\Delta t}{6\Delta x} - \frac{v\Delta t}{6\Delta y} + \frac{1}{6}\left(\frac{u^2\Delta t^2}{\Delta x^2} + \frac{v^2\Delta t^2}{\Delta y^2} + \frac{2D\Delta t}{\Delta x^2} + \frac{2D\Delta t}{\Delta y^2}\right) - \frac{uv\Delta t^2}{4\Delta x\Delta y}\right],\\
\alpha_6 &= \nu\left[-\frac{1}{9} - \frac{u\Delta t}{6\Delta x} - \frac{v\Delta t}{6\Delta y} + \frac{1}{6}\left(\frac{u^2\Delta t^2}{\Delta x^2} + \frac{v^2\Delta t^2}{\Delta y^2} + \frac{2D\Delta t}{\Delta x^2} + \frac{2D\Delta t}{\Delta y^2}\right) + \frac{uv\Delta t^2}{4\Delta x\Delta y}\right],\\
\alpha_7 &= \nu\left[-\frac{1}{9} - \frac{u\Delta t}{6\Delta x} - \frac{v\Delta t}{6\Delta y} + \frac{1}{6}\left(\frac{u^2\Delta t^2}{\Delta x^2} + \frac{v^2\Delta t^2}{\Delta y^2} + \frac{2D\Delta t}{\Delta x^2} + \frac{2D\Delta t}{\Delta y^2}\right) - \frac{uv\Delta t^2}{4\Delta x\Delta y}\right],\\
\alpha_8 &= \nu\left[-\frac{1}{9} + \frac{u\Delta t}{6\Delta x} + \frac{v\Delta t}{6\Delta y} + \frac{1}{6}\left(\frac{u^2\Delta t^2}{\Delta x^2} + \frac{v^2\Delta t^2}{\Delta y^2} + \frac{2D\Delta t}{\Delta x^2} + \frac{2D\Delta t}{\Delta y^2}\right) + \frac{uv\Delta t^2}{4\Delta x\Delta y}\right],\\
\alpha_9 &= \frac{w_e(1-\nu)}{w_e + h\lambda_a}.
\end{aligned}
\tag{C8}
$$

REFERENCES

Alexander, M. A., and C. Deser, 1995: A mechanism for the recurrence of wintertime midlatitude SST anomalies. *J. Phys. Oceanogr.*, **25,** 122–137.

Bathen, K. H., 1972: Heat storage and advection in the North Pacific Ocean. *J. Geophys. Res.*, **76,** 676–687.

Batteen, M. L., C. A. Collins, C. R. Gunderson, and C. S. Nelson, 1995: The effect of salinity on density in the California Current system. *J. Geophys. Res.*, **100,** 8733–8749.

Bendat, J. S., and A. G. Piersol, 1971: *Random Data: Analysis and Measurement Procedures.* Wiley-Interscience, 407 pp.

Cayan, D. R., 1992: Latent and sensible heat flux anomalies over the northern oceans—Driving the sea surface temperature. *J. Phys. Oceanogr.*, **22,** 859–881.

Csanady, G. T., 1978: Turbulent interface layers. *J. Geophys. Res.*, **83,** 2329–2342.

Frankignoul, C., 1985: Sea surface temperature anomalies, planetary waves, and air–sea feedbacks in the middle latitudes. *Rev. Geophys.*, **23,** 357–390.

——, and K. Hasselmann, 1977: Stochastic climate models, Part II: Application to sea-surface temperature anomalies and thermocline variability. *Tellus,* **29,** 289–305.

——, and R. W. Reynolds, 1983: Testing a dynamical model for midlatitude sea surface temperature anomalies. *J. Phys. Oceanogr.*, **13,** 1131–1145.

Hasselmann, K., 1976: Stochastic climate models, Part I: Theory. *Tellus,* **28,** 473–485.

Hasunama, K., and K. Yoshido, 1978: Splitting of the subtropical gyre in the western North Pacific. *J. Oceanogr. Soc. Japan,* **34,** 160–172.

Herterich, K., and K. Hasselmann, 1987: Extraction of mixed layer advection velocities, diffusion coefficients, feedback factors and atmospheric forcing parameters from the statistical analysis of North Pacific SST anomaly fields. *J. Phys. Oceanogr.*, **17,** 2145–2156.

Ichikawa, K., and S. Imawaki, 1994: Life history of a cyclonic ring detached from the Kuroshio Extension as seen by the Geosat altimeter. *J. Geophys. Res.*, **99,** 15 953–15 966.

Imawaki, S., M. Gotoh, H. Yoritaka, N. Yoshioka, and A. Misumi, 1996: Detecting fluctuations of the Kuroshio axis south of Japan using TOPEX/Poseidon altimeter data. *J. Oceanogr.*, **52,** 69–92.

Kelly, K. A., 1989: An inverse model for near-surface velocity from infrared images. *J. Phys. Oceanogr.*, **19,** 1845–1864.

——, and P. T. Strub, 1992: Comparison of velocity estimates from advanced very high resolution radiometer in the coastal transition zone. *J. Geophys. Res.*, **97,** 9653–9668.

Killworth, P. D., D. B. Chelton, and R. A. deSzoeke, 1997: The speed of observed and theoretical long extratropical planetary waves. *J. Phys. Oceanogr.,* **27,** 1946–1966.

Liptser, R. S., and A. N. Shiryayev, 1977: *Statistics of Random Processes* I: *General Theory.* Springer-Verlag, 394 pp.

Lofquist, K., 1960: Flow and stress near an interface between stratified liquids. *Phys. Fluids,* **3,** 158–175.

Maximenko, N. A., G. G. Panteleev, P. P. Niiler, and T. Yamagata, 1999: Near-surface circulation in the north western Pacific. *Int. Symp. Oceanic Fronts and Related Phenomena,* Collected Papers, IOC, UNESCO.

Namias, J., and R. M. Born, 1970: Temporal coherence in North Pacific sea surface temperature patterns. *J. Geophys. Res.,* **75,** 5952–5955.

——, and ——, 1974: Further studies of temporal coherence in North Pacific sea surface temperatures. *J. Geophys. Res.,* **79,** 797–798.

Nitani, H., 1972: Beginning of the Kuroshio. *Kuroshio, Its Physical Aspects,* H. Stommel and Y. Yoshida, Eds., University of Tokyo Press, 129–163.

Ostrovskii, A. G., and L. I. Piterbarg, 1985: Diagnosis of the seasonal variability of water surface temperature anomalies in the North Pacific: Meteorology and hydrology (in Russian). 51–57.

——, and ——, 1995: Inversion for heat anomaly transport from sea surface temperature time series in the northwest Pacific. *J. Geophys. Res.,* **100,** 4845–4865.

——, and ——, 1997: A new method for obtaining velocity and diffusivity from time-dependent distributions of a tracer via the maximum likelihood estimator for the advection-diffusion equation. *J. Comput. Phys.,* **133,** 340–360.

Piterbarg, L. I., 1989: *The Dynamics and Prediction of the Large-Scale SST Anomalies: Statistical Approach* (in Russian). Hydrometeoizdat, Leningrad, 300 pp.

——, and A. G. Ostrovskii, 1997: *Advection and Diffusion in Random Media: Implications for Sea Surface Temperature Anomalies.* Kluwer Academic, 330 pp.

Qiu, B., W. Miao, and P. Muller, 1997: Propagation and decay of forced and free baroclinic Rossby waves in off-equatorial oceans. *J. Phys. Oceanogr.,* **27,** 2405–2417.

Reynolds, R. W., 1978: Sea surface temperature anomalies in the North Pacific Ocean. *Tellus,* **30,** 97–103.

Sverdrup, H. U., M. W. Johnson, and R. H. Fleming, 1946: *The Oceans: Their Physics, Chemistry and General Biology.* Prentice-Hall, 1087 pp.

Tourre, Y. M., and W. B. White, 1995: ENSO signals in global upper-ocean temperature. *J. Phys. Oceanogr.,* **25,** 1317–1332.

White, W. B., and A. E. Walker, 1974: Time and depth scales of anomalous subsurface temperature at ocean weather stations P, N, and V in the North Pacific. *J. Geophys. Res.,* **79,** 4517–4522.

Yasuda, I., K. Okuda, and M. Hirai, 1992: Evolution of a Kuroshio warm-core ring—Variability of the hydrographic structure. *Deep-Sea Res.,* **39** (Suppl.), S131–S161.